# Flexible Superhydrophobic Microlens Arrays for Humid Outdoor Environment Applications

Shiyi Luan, Peng Xu, Yurong Zhang, Longjian Xue,* Yi Song,* and Chengqun Gui*

Cite This: *ACS Appl. Mater. Interfaces* 2022, 14, 53433−53441

Read Online

ACCESS | 📊 Metrics & More | 📰 Article Recommendations | 🔲 Supporting Information

**ABSTRACT:** A microlens array (MLA) is an essential optical imaging device in the applications of augmented and virtual realities. The imaging of MLA would become blurry in a humid outdoor atmosphere. While the incorporation of superhydrophobicity to MLA would prevent the adhesion of droplets, the complex structure and the multiple fabrication process reduce the capability of optical imaging of MLA. Herein, a flexible superhydrophobic MLA with good optical imaging capability is successfully fabricated by the combination of 3D direct laser writing (DLW) and soft lithography. 3D DLW allows the fabrication of MLA with a hierarchical pillar array (h-MLA) in one step, which ensures good optical properties of the resulting polydimethylsiloxane (PDMS) h-MLA. The resulting h-MLAs with pitches ranging between 50 and 100 $\mu$m are superhydrophobic from which water droplets slide away at a sliding angle smaller than 15.6° and bounce off from the surface. Meanwhile, the hierarchical pillar array has a limited impact on the imaging capability and the field of view of h-MLA. With an optimized pitch of 60 $\mu$m, h-MLA has a transparency as good as MLA. Moreover, PDMS h-MLA retains excellent optical and superhydrophobic properties when bent and in an extremely humid environment. We believe that the proposed h-MLA could find applications in outdoor environments.

**KEYWORDS:** superhydrophobic, microlens array, direct laser writing lithography, high filling factor, low roughness
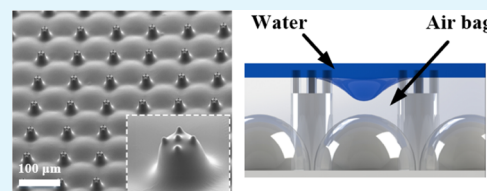
## 1. INTRODUCTION

Based on studies of insect compound eyes, microlens arrays (MLAs) have found applications in many areas, such as fiber coupling, sensing, and beam shaping.[1−6] Due to the rapid development of augmented reality (AR) and virtual reality (VR) technologies, which have applications ranging from daily civil to military applications,[7−11] MLAs are considered indispensable micro-optical devices for virtual imaging.[12−16] For applications in various environments, especially in outdoor environments, composite functions are required for MLAs. For instance, in a humid environment, water droplets could adhere to the MLA surface, which would significantly hinder the imaging performance of the MLA. Therefore, a waterproof function of the MLA is highly required. Meanwhile, the waterproof capability also offers the MLA with a self-cleaning function and enables it to be environment adaptive.[17]

While MLA must have a smooth surface to guarantee transparency, the hydrophobicity, especially the superhydrophobicity, needs the surface to be rough. Two strategies have succeeded in the realization of hydrophobicity MLA.[18,19] One is the direct fabrication of hydrophobic nanostructures on the microlens surface. The improvement in the hydrophobicity by this strategy sacrifices the imaging performance and the transparency due to light scattering.[20] Alternatively, motivated by the waterproof microstructures in biological ommatidia and plants, researchers added hydrophobic microstructures,[20,21] such as micropillars, between microlenses to endow an MLA with a waterproof property.[22−26] Such an MLA is a hybrid

pattern composed of two types of microstructures: hydrophobic microstructures with rough surfaces and microlenses with smooth surfaces. In this case, the MLA retains good imaging performance. Nevertheless, to meet the requirements of the two paradoxical characteristics, a combination of multiple technologies is usually used to prepare waterproof MLA structures. Recently, Li et al.[21] achieved a superhydrophobic MLA structure, which was obtained by three manufacturing technologies, photolithography, microprinting, and chemical growth. In this approach, a photomask is generally needed, and the precise alignment between the MLA and hydrophobic microstructures is highly required. To avoid alignment error, the spaces between the hydrophobic structures and microlenses should be sufficiently large,[18,20,21,26] which undoubtedly sacrifices the filling factor of the MLA, leading to a reduction in the information acquisition and imaging capability.[27] Additionally, the complex fabrication processes also reduced their choice of substrate materials, hence flexible MLA is difficult to prepare.[27]
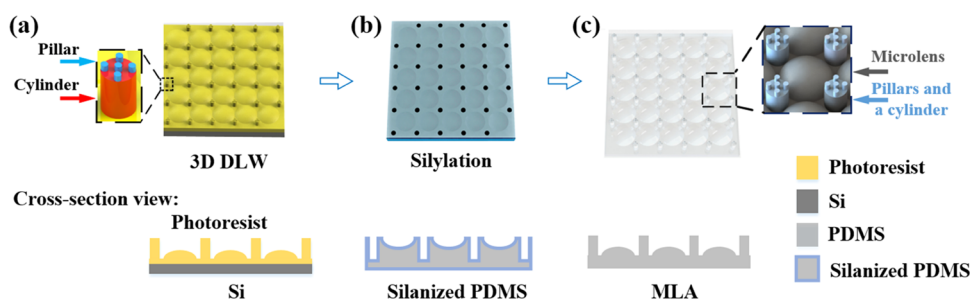
Here, an MLA and superhydrophobic microstructures were constructed within one step without the requirement of a
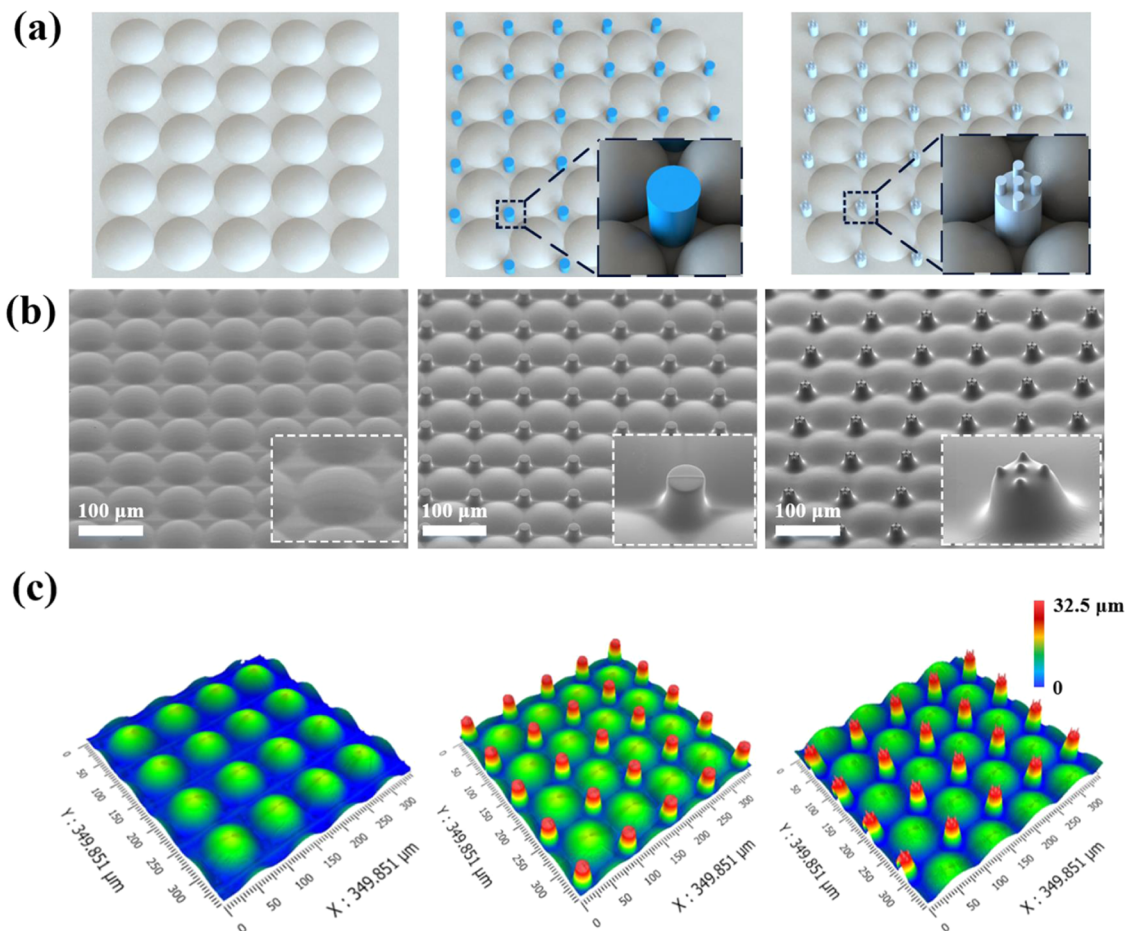
**Figure 1.** Schematic illustration of the fabrication of a flexible MLA with microstructures: (a) 3D DLW to prepare an MLA with microstructures made of PR within one step. Inset: A microstructure composed of pillars and a cylinder. (b) Silanization of the negative mold. (c) Flexible MLA with microstructures after the second soft lithography process.



**Figure 2.** (a) Schematic illustrations, (b) SEM and (c) 3D images of n-MLA (left), c-MLA (middle), and h-MLA (right) made of PDMS. The insets in (a, b) are (a) magnified schematic illustrations and (b) magnified SEM images of the MLA, cylinder, and hierarchical pillar, respectively.

photomask, making use of 3D direct laser writing (DLW). This method significantly reduces the fabrication complexity and allows us to conveniently optimize the functions by regulating the structure parameters due to the high fabrication freedom by DLW. By employing soft lithography, the MLA with a hierarchical pillar array (h-MLA) was successfully transferred to a flexible material, polydimethylsiloxane (PDMS). The hierarchical pillar array offers the resulting PDMS h-MLA with a water contact angle (CA) of 151.8° and a sliding angle (SA) lower than 5.8°. Although the existence of a hierarchical pillar array, superhydrophobic MLA, which has a filling factor of 78%, achieves a transmissivity of 92.3%, close to the normal MLA (n-MLA), the superhydrophobic h-MLA exhibits great

potential in waterproof applications in humid environments, and the flexibility provides a wide application prospect in the field of the flexible display.

## 2. RESULTS AND DISCUSSION

**2.1. Design and Fabrication.** Generally, three types of MLAs with different filling factors are used as components of optical devices: a fully packed array, a close-packed array, and a rectangular array. The corresponding filling factors are 100, 90.7, and 78%, respectively. To integrate microstructures between the microlenses and realize superhydrophobicity, an MLA with a 78% filling factor was selected. The hydrophobic microstructure was fabricated in the remaining area (22%).

Two types of hydrophobic microstructures were designed: a cylinder array and a hierarchical structure with five secondary tiny pillars on top of the cylinders, which are expected to bring hydrophobicity to the surface.[28−31]

3D DLW technology was carried out to generate designed structures in the spin-coated photoresist on a Si substrate. Through the grayscale exposure and development to the photoresist, the desired pattern of h-MLA was achieved (Figure 1a). The photoresist pattern was then transferred into a negative PDMS mold (Figures 1b and S1a) and then to the final structure upon the second replication (Figure 1c).

To realize the superhydrophobicity, a high microstructure is preferred. However, the structural size is limited by the deep of field (DOF) of the 3D DLW, which determines the maximum height of 32 μm and a height-to-width ratio of 1.2:1. Therefore, all of the cylinders were designed to be 26 μm in height and diameter; all of the secondary pillars were designed to be 6 μm in height and diameter, respectively (Figure 2a, Table 1). In this study, three different types of MLA were

**Table 1. Diameter of the Cylinders and Pillars and the Height-to-Diameter Ratio of the Microstructures**

| microstructure type | diameter of the cylinders (μm) | diameter of the pillars (μm) | height-to-diameter ratio |
|---|---|---|---|
| n-MLA | | | |
| c-MLA | 26 | | 1.0 |
| h-MLA | 26 | 6 | 1.2 |

compared: n-MLA, MLA with cylinders among microlenses (c-MLA), and h-MLA (Figures 2b,c and S2). Typically, an area of 30 × 30 mm² was conveniently realized in one step (Figure S3), and the generation of stress in the conventional multiple-step process was avoided.[32]

**2.2. Hydrophobicity.** To examine the wettability of the fabricated MLAs with different microstructures, the dynamic and static characteristics of water droplets on the h-MLA were investigated. The h-MLA at a pitch of 80 μm has a CA of 153°; hence, it is superhydrophobic (Figure 3a). For a water droplet dropped on h-MLA (Figure 3b), the spreading time of the drop was 3.37 ms. Then, at 8.62 ms, the water droplet started to retract, reaching the highest point at 26.5 ms (Supplementary Video 1). Based on the Cassie−Baxter theory, the height of the air−liquid interface between the water and "airbag" determines the MLA hydrophobicity.[20] In this design, the pillars on the cylinder structures enhance the height of the air−liquid interface and reduce the contact area between the droplets and microstructures (Figure 3c), which endows the h-MLA with superhydrophobicity. In comparison, the CA of c-MLA was 141°, much lower than that of h-MLA (Figure 3d). For the water droplet dropping on c-MLA (see Supplementary Video 2), the spreading time and retraction time were 4.16 and 6.00 ms, respectively. The droplet left c-MLA at a contact time of 29.25 ms (Figure 3e), which was longer than that on h-MLA. Owing to the tiny pillars designed in h-MLA, the solid−liquid contact area was reduced, which induced the elevation of the air−liquid interface height. Meanwhile, the pillars reduced the contact area and thus the adhesion force between the droplet and h-MLA, providing more kinetic energy to lift water droplets. In contrast, the cylinder top provides a larger contact area for the droplet. Moreover, a smaller "airbag" between the water droplet and c-MLA may induce contact between the liquid and the microlenses, further increasing the adhesion force (Figure 3f). For the n-MLA, the water droplet on the surface has the lowest CA = 107° (Figure 3g), so the dropping droplet would not leave the n-MLA surface (Figure 3h). Unlike h-MLA or c-MLA, there was no "airbag" between the liquid and the microlenses in n-MLA (Figure 3i), resulting in
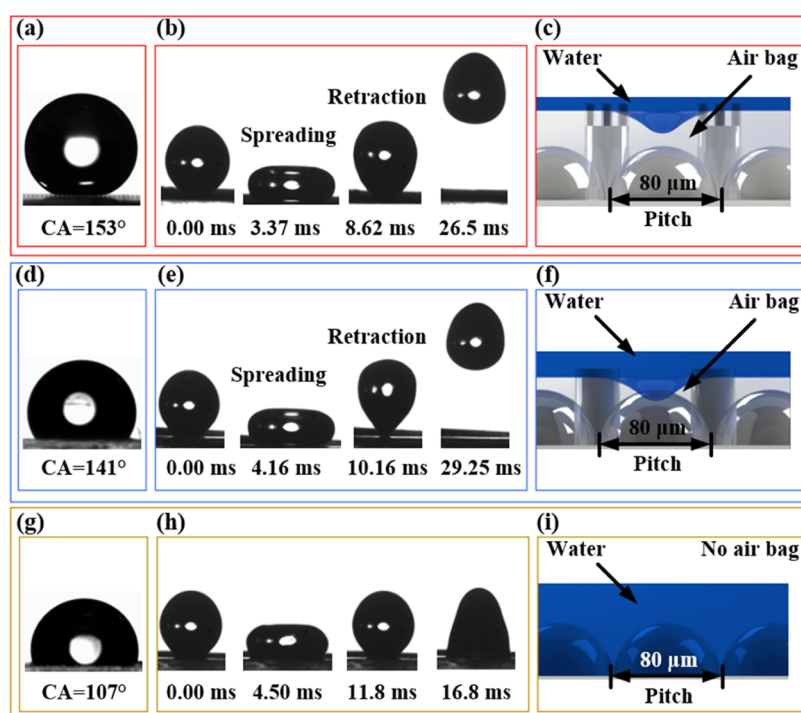


**Figure 3.** (a, d, g) CA; (b, e, h) dynamic behavior (selected moments captured using a high-speed camera); and (c, f, i) schematic depictions of a water droplet on (a−c) h-MLA, (d−f) c-MLA, and (g−i) n-MLA, respectively.
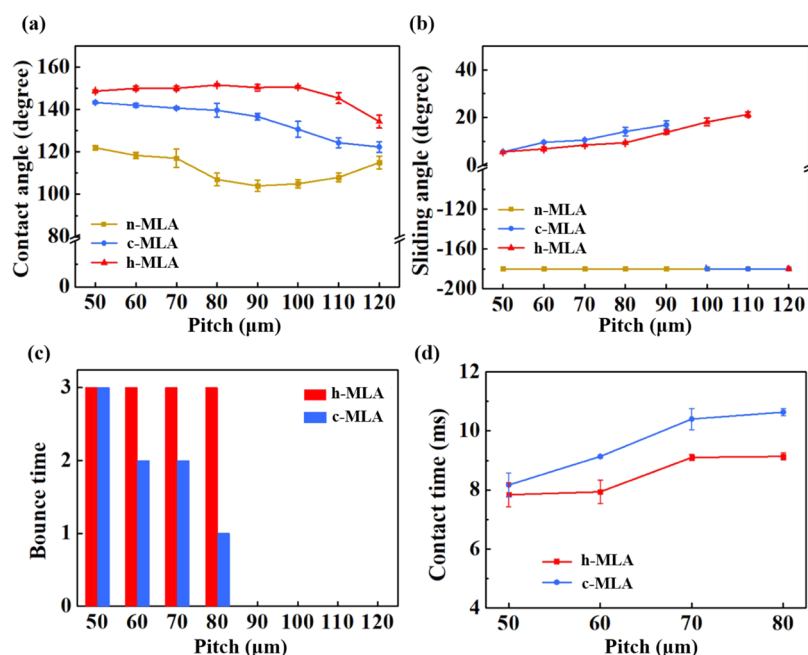
**Figure 4.** Dependence of (a) contact angle and (b) sliding angle on the pitch size of n-MLA, c-MLA, and h-MLA, respectively. Dependence of (c) bounce time and (d) contact time on the pitch size of c- and h-MLA.
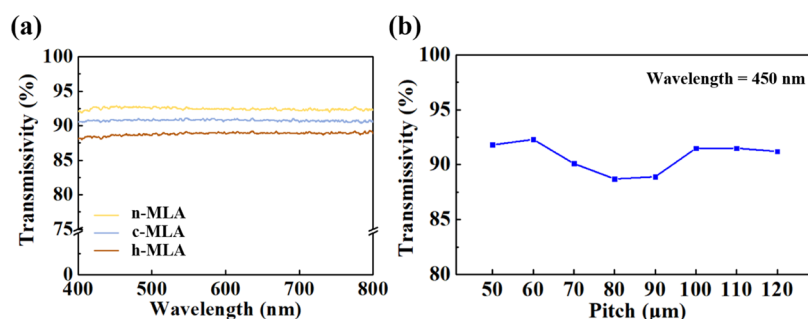


**Figure 5.** (a) Transmittance of three types of MLA with a pitch size of 80 $\mu$m. (b) Influence of the pitch size on the transmittance at a wavelength of 450 nm of h-MLA.

the adhering of water droplets on the surface (see Supplementary Video 3).

The influence of the MLA pitch on the CA of h-MLA was further investigated (Figure 4a). When the pitch ranged from 50 to 100 $\mu$m, CAs on h-MLAs were ~151°. For the construction of bioinspired superhydrophobic surfaces, it is very well accepted that the combination of micro- and nanostructures is essential for achieving a water CA larger than 150° (and as close as possible to 180°).[33,34] On the other hand, the nanostructure is not strong enough to stand rough conditions. Here, we sacrificed part of the superhydrophobicity, with the water CA just slightly larger than 150°, which can still be regarded as a superhydrophobic surface. The secondary pillars, which are also on microscale, decreased the contact area between the microstructures and water, hindering the contact between water droplets and microlenses. As a result, the small area of water droplets contacting the microlenses contributes to a higher CA. h-MLAs with the pitch ranging from 50 to 100 $\mu$m exhibit little difference in hydrophobicity, suggesting a high tolerance to the dimension design. h-MLAs with an increasing pitch beyond 100 $\mu$m have weakened hydrophobicity, where the CA gradually decreased to 137° at a pitch of 120 $\mu$m, which can be attributed to the

gradually increased gaps between cylinders. In contrast, the CA of the water droplet on the n-MLA surfaces is lower than 120°, even smaller than that of c-MLAs.

Moreover, SAs of h-MLAs were also measured (Figure 4b). For some superhydrophobic surfaces, water droplets would slide away when the surface was turned upside down, and the SA can be regarded as 180° (or close to 180°). To distinguish from these surfaces, we thus define the surfaces, on which water droplet sticks to the surface even when the surface is turned upside down, with an SA of −180°.[35] The SA on c-MLA increased from 5.7 to 16.8° with the increase of the pitch. The water droplet on the c-MLAs with pitches beyond 90 $\mu$m cannot roll off. When combined with pillars, SAs of h-MLA were smaller than that of c-MLA. Water droplets can still slide away even if the pitch was increased to 100 $\mu$m. In the case of n-MLAs, water droplets kept sticking to the surface regardless of the pitch.

To understand the impact of the pillar on the dynamic behavior of water droplets, the bounce times of the water droplets dropping on MLAs with different structures were compared (Figure 4c). When the pitch was in the range between 50 and 80 $\mu$m, the water droplets bounced three times on the surface of h-MLAs. In contrast, the bounce time on the
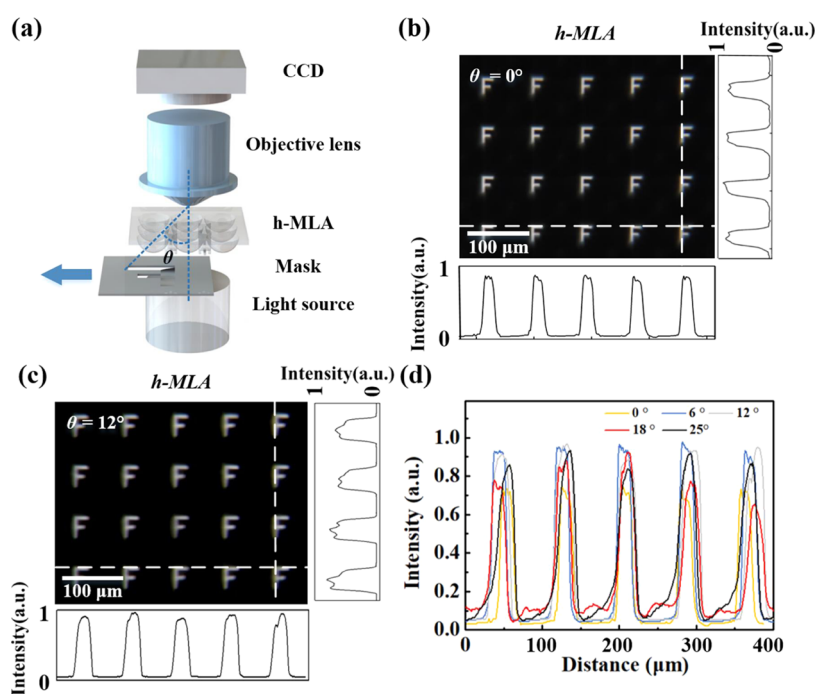
**Figure 6.** (a) Schematic diagram of the experimental setup to test the effect of the inclined illumination angle ($\theta$) on the imaging function of flexible h-MLA. (b, c) Typical images obtained from the flexible h-MLA with $\theta$ of (b) 0° and (c) 12°, respectively. Insets in (b, c) show the corresponding intensity cross sections. (d) Intensity cross sections of images obtained under various $\theta$s.

c-MLAs decreases from 3 to 1 when the pitch increases from 50 to 80 $\mu$m. It suggests that the increasing pitch reduces the kinetic energy to lift the droplet up,[36] and it also proves that the integration of the pillars on the cylinders improves the waterproof performance. On increasing the pitch to 90 $\mu$m, water droplets did not bounce off from n-MLA and c-MLA, which indicates that the capillary force and kinetic energy are not enough to lift the droplet up.[37,38] It also infers that the kinetic-energy reduction upon increasing the pitches is greater than the increase of kinetic energy induced by the addition of pillars on top of cylinders. Furthermore, the contact time of water droplets dropping on MLAs was investigated (Figure 4d). The contact time of the water droplet on h-MLA was shorter than that on c-MLAs regardless of the pitch. The result proves that the water droplets dropping on h-MLAs have larger capillary forces, which gives more kinetic energy to lift them up.

**2.3. Optical Imaging Properties.** Light transmittance has a vital impact on the imaging function of optical elements. To evaluate the influence of a superhydrophobic structure on the transmittance of MLA, the spectral transmittances of different PDMS MLAs over the visible spectrum were measured (Figure 5a). n-MLA with a pitch of 80 $\mu$m has a transmittance of over 92.7% with the light wavelength ranging from 400 to 800 nm. The transmittance of n-MLA reached 92.7%, which could be induced by the collecting light function of microlens with a high numerical aperture. The incorporation of hydrophobic components (cylinders with a diameter of 26 $\mu$m and a height of 26 $\mu$m) to n-MLA reduced the transmittance at 450 nm from 92.7 to 90.8%, while the incorporation of super-hydrophobic components (cylinders with a diameter of 26 $\mu$m and a height of 26 $\mu$m and pillars with a diameter of 6 $\mu$m and a height of 6 $\mu$m) further reduced the transmittance to 88.6%. It is reasonable that the incorporation of pillar-like

structures among MLA would scatter some light and reduces the transmittance.

The influence of the structure size on the transmittance of h-MLA was further tested (Figure 5b). h-MLA with a pitch of 50 $\mu$m has a transmittance of 91.8% at a wavelength of 450 nm. The increase of the pitch to 60 $\mu$m increased the transmittance to 92.3%, quite close to n-MLA. The further increase in the pitch to 80 $\mu$m, however, greatly reduced the transmittance to 88.6%. The transmittance recovered to above 91.2% once the pitch was larger than 100 $\mu$m. It indicates that, with an optimal pitch size, the transmission of the designed h-MLA can be as high as an n-MLA, fully meeting the imaging demands in various application scenarios.[39−41]

By importing superhydrophobic structures into the MLA, the waterproof performance was significantly improved. However, the superhydrophobic microstructures are expected to have some impact on the imaging performance of MLAs.[42−44] The influence of the inclined illumination angle ($\theta$), which is defined as the angle between the visual range edge and the optic axis of the MLA, on the imaging function was then investigated (Figure 6a). $\theta$ was changed by gradually pulling the mask "F" to the visual range edge of the MLA. The theoretical max value of $\theta$ is the field of view (FOV) of the microlens, which can be calculated via the following equation[45]

$$FOV = 2\arccos\frac{R - H}{R} \tag{1}$$

where $H$ and $R$ are the sagittal height and the radius of the MLA, respectively. As the theoretical FOV of n-MLA is 52°, the theoretical maximum $\theta$ is 26° due to the symmetrical structure of the microlenses. The contrasts of images were also calculated

$$contract = \frac{I_{max} - I_{min}}{I_{max} + I_{min}} \tag{2}$$
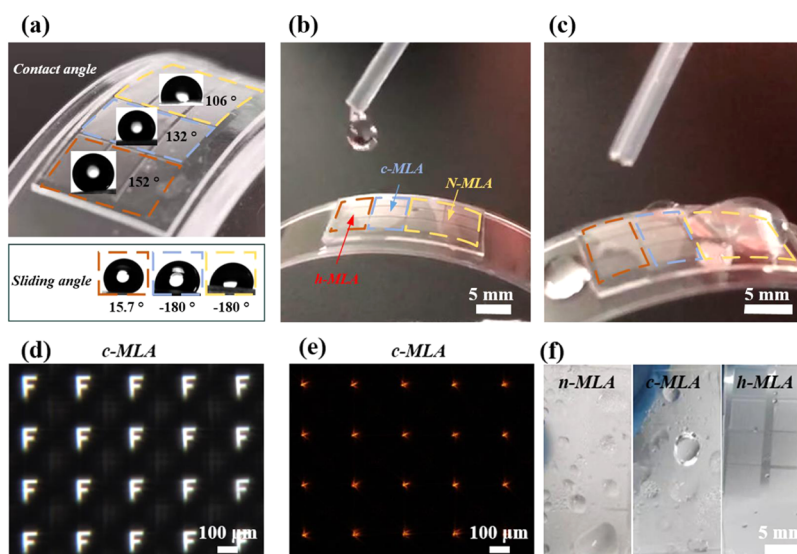
**Figure 7.** (a) Optical photos of a bent flexible h-MLA, a bent flexible c-MLA, and a bent flexible n-MLA (colored red, blue, and yellow, respectively). Inset: Shapes of water droplets on the three types of bent MLAs and their corresponding CA and SA. (b) Optical photo of dripping water on the three types of bent MLAs. (c) Optical photo of the three types of bent MLAs after dripping water. (d) Images obtained from the bent h-MLA after dripping water. (e) Focusing performance of the bent h-MLA after dripping water onto it. (f) Snapshots showing the waterproof experiments of three types of MLAs in a humid outdoor environment.

The insets show the corresponding intensity cross sections. $I_{max}$ represents the max intensity of the image and $I_{min}$ represents the min intensity of the image. Under normal illumination, $\theta = 0°$, the h-MLA with a pitch size of 80 $\mu$m showed a clear image and had a contrast of 0.89, which is quite close to that of n-MLA (0.90) and h-MLA (0.90) (Figures 6b and S4). Increasing $\theta$ will lead to a blurring of the obtained image. Although the pattern "F" could be clearly detected in a large FOV, the blurring of the image became stronger when $\theta$ increased (Figures 6c and S5). The intensity distributions of images with $\theta$ of 0, 6, and 12° exhibited very sharp edges, which got smoother when $\theta$ was 18 and 25° (Figure 6d). However, the image formed by the n-MLA with $\theta$ up to 25° was not affected (Figure S6). It indicates that cylinders and pillars have a negative impact on imaging performance under inclined illuminations. Nevertheless, the image pattern can still be easily recognized; hence, the h-MLA retains a good imaging function and wide FOV.

**2.4. Optical Imaging Properties in a Humid Environment.** PDMS h-MLA is suitable for applications that require deformations in practice. The waterproof and imaging functions of the h-MLA under bending were thus tested to study. The sample was placed on a circular substrate with a diameter of 50 mm to simulate the bending state (Figure 7a). To compare the difference originating from the microstructures, h-MLA, c-MLA, and n-MLA were fabricated on one substrate for the sake of process consistency, eliminating the interference due to the process differences. The water droplet on the bent h-MLA has a CA of 152°, showing good hydrophobicity. In contrast, the CAs of c-MLA and n-MLA are 132 and 106°, respectively, exhibiting relatively weak hydrophobicity (insets in Figure 7a). Meanwhile, only the water droplet on the surface of h-MLA can slide away at a SA of 15.7°, while water droplets stuck on the other two MLAs with SA noted as −180°. When the curvature of MLA increased from 0 to 0.2, the SA on the h-MLA increased from 9.7 to 15.7°. It has been argued that the increase in the curvature increases the pitch of the upper end of the microstructures,

which decreases the hydrophobicity performance.[38] In contrast, increasing the curvature of c-MLA to 0.2 enables the water droplets to stuck on the surface (SA noted as −180°) (insets in Figure 7a). It is thus inferred that the flexible electronic display screen equipped with the h-MLA would retain a good waterproof performance with a curvature of up to 0.2. Moreover, water was dripped on the surface of bent samples to investigate the waterproof function (Figure 7b). The dropped water droplet did not adhere to the flexible h-MLA but adhered to n-MLA and partially adhered to c-MLA (Figure 7c). Since no water droplet adhered to the h-MLA surface, the quality of the images gained by h-MLA was not affected (Figure 7d,e). With an ambient humidity of 100% produced by a humidifier (Figure S8), water droplets condensed on the surfaces of c-MLA and n-MLA and remained on the surfaces. In contrast, the condensed water droplets on h-MLA slipped off without any residual droplets (Figure 7f). The tests of immersing in water for 30 s also demonstrated the better waterproof function of h-MLA (Figure S9). It suggests that h-MLA has excellent adaptability to the extremely humid environment. Thus, the flexible h-MLA exhibited a much better imaging performance in humid environments.

It is well known that durability is a very critical issue for superhydrophobic materials. To test the durability, h-MLA was bent and kneaded 30 times, and it was also rubbed on the surface with dust. After the above process, the water CA of the h-MLA surface remained at 151°, suggesting good durability of h-MLA (Figure S10).

## 3. CONCLUSIONS

In summary, a convenient fabrication method, 3D DLW technology, was used to construct an MLA with a hierarchical pillar array (h-MLA) within one step. For h-MLA with pitches ranging from 50 to 100 $\mu$m, CAs were larger than 151°, and the SAs were smaller than 15.6°. Meanwhile, the transmittance reached 92.3%, close to n-MLA. The superhydrophobic structure not only enabled falling water droplets to quickly

leave the surface but also showed almost no effect on the imaging quality and FOV. Moreover, MLA retained excellent superhydrophobic and imaging functions when it was bent or in an extremely humid environment. We believe the h-MLA proposed here could find applications in real practice.

## 4. EXPERIMENTAL SECTION

The main fabrication process of the h-MLA includes two steps: a 3D DLW process and a PDMS replication process. 3D DLW process: A PR (Merck, AZ4562) was spin-coated on a Si substrate with a thickness of 1 mm. It was spin-coated at a speed of 750 rpm for 20 s and relaxed for 20 min. Then, the PR was spin-coated again on top of the first PR layer at a speed of 650 rpm for 20 s, followed by a 20 min relaxation and a 40 min soft bake to solidify the PR. Subsequently, DLW technology (4PICO, Pico Master 100) was directly used to perform grayscale exposure of the PR. The exposure dose was 1500 mJ/mm$^2$. The working laser spot was 800 nm. The working speed of the laser spot was 100 mm/s. The offset of the focus depth was 0 $\mu$m. At a ratio of 3:1 (by weight), ultrapure water was mixed with the developer (AZ 400K). The developing time was 8 min. The acquired MLA was baked for 20 s at 90 °C. PDMS replication process: A PDMS elastomer kit (Sylgard 184) was purchased from Dow Corning (MI). At a ratio of 10:1 (by weight), the PDMS prepolymer was mixed with the cross-linker and degassed for 10 min at 60 °C. The mixture was poured onto the PR, followed by curing at 60 °C for 3 h (Figure S1a). After peeling off the PDMS mixture from the PR, a negative mold was acquired, and it was placed on glass (Figure S1b). Then, the PDMS mold was coated with 1H,1H,2H,2H perfluorodecyltriethoxysilane after plasma treatment with an oxygen ion.[30] The PDMS mold coated with 1H,1H,2H,2H perfluorodecyltriethoxysilane was placed in a vacuum environment for 40 min and was coated with the PDMS mixture again. Next, the silanized negative mold was spin-coated with 1 mm thick PDMS, and a second hot-curing process was employed on the negative mold to realize pattern replication (Figure S1c). The negative mold with PDMS was placed in an oven again at 60 °C for 3 h to realize curing. After peeling the PDMS film from the negative mold (Figure S1d), the fabrication of the h-MLA was completed (Figure 1d). Notably, since the PDMS mold was coated with 1H,1H,2H,2H perfluorodecyltriethoxysilane after plasma treatment with an oxygen ion, hence perfluorodecyltriethoxysilane was adhesive on the PDMS mold. Therefore, there is little perfluorodecyltriethoxysilane on the surface of the prepared MLA.

Characterization: SEM images of the gold-sputtered samples were taken by a field-emission scanning electron microscope (Tescan, Brno, s.r.o.). Sample profiles and morphologies were measured by a white light interferometer (ZYGO, Nexview). The transmittance of the samples was measured by a UV spectrophotometer (Lambda 365 UV−Vis spectrophotometer, Perkin Elmer). The components of the optical measurement system included an objective lens (Daheng, GCO-2107), two light sources (Thorlab, CPS635; Lemons, KM-FL2929), and a charge-coupled device (CCD) (Daheng, MER-2000-19U3C-L). Two three-dimensional motion platforms (Daheng, GCM-901602M) were used to adjust the distance between the object and the image.

## ASSOCIATED CONTENT

### ⓢ Supporting Information

The Supporting Information is available free of charge at https://pubs.acs.org/doi/10.1021/acsami.2c17128.

> Fabrication process of the MLA (Figure S1); profiles of the microlens, cylinder structure, and cylinder with hierarchical pillar array (Figure S2); photo of a 30 × 30 mm$^2$ microstructure fabricated by 3D DLW technology (Figure S3); schematic diagram of the experimental setup for MLA imaging and images obtained from flexible n-MLA and flexible c-MLA (Figure S4); images

obtained from flexible h-MLA with $\theta$ of 6, 18, and 25°, respectively, and insets show the corresponding intensity cross sections (Figure S5); image formed by the n-MLA with inclined illumination ($\theta$ = 25°) (Figure S6); physical figure of the three different MLAs on a curved substrate (Figure S7); three types of MLAs before waterproof experiments and three types of MLAs in the process of the waterproof experiments (Figure S8); experiments to test the waterproof function of the three types of MLAs after immersing them in water for 30 s (Figure S9); and durability test experiments of the h-MLA (Figure S10) (PDF)

Water droplet started to retract, reaching the highest point at 26.5 ms (MP4)

Water droplet dropping on c-MLA (MP4)

Adhering of water droplets on the surface (MP4)

## AUTHOR INFORMATION

### Corresponding Authors

**Longjian Xue** − *School of Power and Mechanical Engineering, Wuhan University, Wuhan 430072, China; The Institute of Technological Sciences, Wuhan University, Wuhan 430072, China;* ⓞ orcid.org/0000-0001-5512-747X; Email: xuelongjian@whu.edu.cn

**Yi Song** − *The Institute of Technological Sciences and School of Microelectronic, Wuhan University, Wuhan 430072, China;* ⓞ orcid.org/0000-0001-9632-404X; Email: yi.song@whu.edu.cn

**Chengqun Gui** − *The Institute of Technological Sciences, Wuhan University, Wuhan 430072, China;* Email: cheng.gui@whu.edu.cn

### Authors

**Shiyi Luan** − *School of Power and Mechanical Engineering, Wuhan University, Wuhan 430072, China;* ⓞ orcid.org/0000-0001-6334-6058

**Peng Xu** − *School of Power and Mechanical Engineering, Wuhan University, Wuhan 430072, China*

**Yurong Zhang** − *The Institute of Technological Sciences, Wuhan University, Wuhan 430072, China*

Complete contact information is available at:
https://pubs.acs.org/10.1021/acsami.2c17128

### Notes

The authors declare no competing financial interest.

## REFERENCES

(1) Jiang, P.; McFarland, M. J. Wafer-Scale Periodic Nanohole Arrays Templated from Two-Dimensional Nonclose-Packed Colloidal Crystals. *J. Am. Chem. Soc.* **2005**, *127*, 3710−3711.

(2) Sohn, I.-B.; Choi, H.-K.; Noh, Y.-C.; Kim, J.; Ahsan, M. S. Laser Assisted Fabrication of Micro-Lens Array and Characterization of their Beam Shaping Property. *Appl. Surf. Sci.* **2019**, *479*, 375−385.

(3) Cheng, Y.-C.; Chen, C.-C.; Hsu, W.-Y.; Wang, P. J.; Tsai, D. P.In The Fabrication of High Filling Factor Double Side Micro Lens Array with High Alignment Accuracy, *SPIE Optical Engineering +*

*Applications, Optical Manufacturing and Testing IX*, San Diego, United States, 27 September, 2011.

(4) Lin, V.; Wei, H.-C.; Hsieh, H.-T.; Su, G.-D. J. An Optical Wavefront Sensor Based on a Double Layer Microlens Array. *Sensors* **2011**, *11*, 10293−10307.

(5) Kumar, M. S.; Sharma, R.; Narayanamurthy, C. S.; Kumar, A. S. K. Determination of the Focal Length of Microlens Array by Spherical Wavefronts. *Opt. Eng.* **2014**, *53*, No. 064102.

(6) Yu, X.-H.; Wang, Z.; Han, Y.-C. Microlenses Fabricated by Discontinuous Dewetting and Soft Lithography. *Microelectron Eng.* **2008**, *85*, 1878−1881.

(7) Chen, S. H.; Yi, X. J.; Li, Y.; He, M.; Chen, S. X.; Kong, L. B.Design of Diffractive Microlens Array Integration with Focal Plane Arrays, *Optics and Optoelectronic Inspection and Control: Techniques, Applications, and Instruments, Biomedical Photonics and Optoelectronic Imaging*, Beijing, China, 5 November, 2000.

(8) Pang, Y. F.; Xu, C. T.; Cao, A.; Shi, L. F.; Fu, Y.; Pang, Hu.; Deng, Q. L.; Liu, L. W.; Liu, W. J.Light Field Acquisition using Microlens based on 3ds Max and Image Reconstruction Technology, *SPIE/COS Photonics Asia, Advanced Optical Imaging Technologies*, 2018.

(9) Colonnier, F.; Manecy, A.; Juston, R.; Viollet, S.In Visual Odometry and Low Optic Flow Measurement by Means of a Vibrating Artificial Compound Eye, In *Conference on Biomimetic and Biohybrid Systems 4th International Conference, Living Machines*, Barcelona, Spain, July 28−31, 2015.

(10) Li, J.; Wang, W.; Mei, X.; Hou, D.; Pan, A.; Liu, B.; Cui, J. Fabrication of Artificial Compound Eye with Controllable Field of View and Improved Imaging. *ACS Appl. Mater. Interfaces* **2020**, *12*, 8870−8878.

(11) Yuan, S.; Yin, J.; Jin, J.; Song, L.; Ma, J.; Yan, S.; Luan, S. Facile fabrication of Microsphere-polymer Brush Hierarchically Three-dimensional (3D) Substrates for Immunoassays. *Chem. Commun.* **2015**, *51*, 6749−6752.

(12) McIntire, J. P.; Havig, P. R.; Geiselman, E. E. Stereoscopic 3D displays and Human Performance: A Comprehensive Review. *Displays* **2014**, *35*, 18−26.

(13) Muthe, L. P.; Pickering, P. K.; Gauss, C. A Review of 3D/4D Printing of Poly-Lactic Acid Composites with Bio-Derived Reinforcements. *Compos., Part C: Open Access* **2022**, *8*, No. 100271.

(14) Zhu, Y. Z.; Tang, T. T.; Zhao, S. Y.; Joralmon, D.; Poit, Z.; Ahire, B.; Keshav, S.; Raje, A. R.; Blair, J.; Zhang, Z. L.; Li, X. J. Recent Advancements and Applications in 3D printing of Functional Optics. *Addit. Manuf.* **2022**, *52*, No. 102682.

(15) Ratcliff, J.; Supikov, A.; Alfaro, S.; Azuma, R. ThinVR: Heterogeneous Microlens Arrays for Compact, 180 degree FOV VR Near-eye Displays. *IEEE Trans. Visual. Comput. Graph.* **2020**, *26*, 1981−1990.

(16) Darkhanbaatar, N.; Erdenebat, M.-U.; Shin, C.-W.; Kwon, K.-C.; Lee, K.-Y.; Baasantseren, G.; Kim, N. Three-dimensional Aee-through Augmented-reality Display System using a Holographic Micromirror Array. *Appl. Opt.* **2021**, *60*, 7545−7551.

(17) Neinhuis, C.; Barthlott, W. Characterization and Distribution of Water-repellent, Self-cleaning Plant Surfaces. *Ann. Bot.* **1997**, *79*, 667−677.

(18) Zheng, L.; Zhang, Y.; Lin, H.; Kang, S.; Li, Y.; Sun, D.; Chen, M.; Wang, Z.; Jiao, Z.; Wang, Y.; Dai, B.; Zhuang, S.; Zhang, D. Ultrasound and Near-Infrared Light Dual-Triggered Upconversion Zeolite-Based Nanocomposite for Hyperthermia-Enhanced Multi-modal Melanoma Therapy via a Precise Apoptotic Mechanism. *ACS Appl. Mater. Interfaces* **2020**, *12*, 32420−32431.

(19) Yong, J.; Bian, H.; Yang, Q.; Hou, X.; Chen, F. Mini-Review on Bioinspired Superwetting Microlens Array and Compound Eye. *Front. Chem.* **2020**, *8*, No. 575786.

(20) Li, M.; Yang, Q.; Chen, F.; Yong, J.; Bian, H.; Wei, Y.; Fang, Y.; Hou, X. Integration of Great Water Repellence and Imaging Performance on a Superhydrophobic PDMS Microlens Array by Femtosecond Laser Microfabrication. *Adv. Eng. Mater.* **2019**, *21*, No. 1800994.

(21) Li, J.; Wang, W.; Mei, X.; Pan, A. Designable Ultratransparent and Superhydrophobic Surface of Embedded Artificial Compound Eye with Extremely Low Adhesion. *ACS Appl. Mater. Interfaces* **2020**, *12*, 53557−53567.

(22) Koch, K.; Bhushan, B.; Barthlott, W. Diversity of Structure, Morphology and Wetting of Plant Surfaces. *Soft Matter* **2008**, *4*, 1943−1963.

(23) Koch, K.; Bhushan, B.; Barthlott, W. Multifunctional Surface Structures of Plants: An Inspiration for Biomimetics. *Prog. Mater. Sci.* **2009**, *54*, 137−178.

(24) Sun, T.; Feng, L.; Gao, X.; Jiang, L. Bioinspired Surfaces with Special Wettability. *Acc. Chem. Res.* **2005**, *38*, 644−652.

(25) Dong, Y.; Ma, L.; Tang, C. Y.; Yang, F.; Quan, X.; Jassby, D.; Zaworotko, M. J.; Guiver, M. D. Stable Superhydrophobic Ceramic-Based Carbon Nanotube Composite Desalination Membranes. *Nano Lett.* **2018**, *18*, 5514−5521.

(26) Wu, D.; Wang, J.-N.; Niu, L.-G.; Zhang, X. L.; Wu, S. Z.; Chen, Q.-D.; Lee, L. P.; Sun, H. B. Bioinspired Fabrication of High-Quality 3D Artificial Compound Eyes by Voxel-Modulation Femtosecond Laser Writing for Distortion-Free Wide-Field-of-View Imaging. *Adv. Opt. Mater.* **2014**, *2*, 751−758.

(27) Liu, F.; Yang, Q.; Chen, F.; Zhang, F.; Bian, H.; Hou, X. Low-cost High Integration IR Polymer Microlens Array. *Opt. Lett.* **2019**, *44*, 1600−1602.

(28) Park, Y.-B.; Im, M.; Im, H.; Choi, Y.-K. Superhydrophobic Cylindrical Nanoshell Array. *Langmuir* **2010**, *26*, 7661−7664.

(29) Nosonovsky, M.; Bhushan, B. Biomimetic Superhydrophobic Surfaces: Multiscale Approach. *Nano Lett.* **2007**, *7*, 2633−2637.

(30) Yeh, K.-Y.; Chen, L.-J.; Chang, J.-Y. Contact Angle Hysteresis on Regular Pillar-like Hydrophobic Surfaces. *Langmuir* **2008**, *24*, 245−251.

(31) Li, Q.; Li, L.; Shi, K.; Yang, B.; Wang, X.; Shi, Z.; Tan, D.; Meng, F.; Liu, Q.; Hu, S.; Lei, Y.; Liu, S.; Xue, L. Reversible Structure Engineering of Bioinspired Anisotropic Surface for Droplet Recognition and Transportation. *Adv. Sci.* **2020**, *7*, No. 2001650.

(32) Li, W.; Yu, M.; Sun, J.; Mochizuki, K.; Chen, S.; Zheng, H.; Li, J.; Yao, S.; Wu, H.; Ong, B. S.; Kawata, S.; Wang, Z.; Ren, K. Crack Engineering for the Construction of Arbitrary Hierarchical Architectures. *Proc. Natl. Acad. Sci. U.S.A.* **2019**, *116*, 23909−23914.

(33) Su, B.; Guo, W.; Jiang, L. Learning from Nature: Binary Cooperative Complementary Nanomaterials. *Small* **2015**, *11*, 1072−1096.

(34) Yao, X.; Song, Y.; Jiang, L. Applications of Bio-Inspired Special Wettable Surfaces. *Adv. Mater.* **2011**, *23*, 719−734.

(35) Shi, K.; Li, Q.; Zhang, J.; Li, L.; Yang, B.; Hu, S.; Lei, Y.; Liu, Z.; Liu, S.; Xue, L. J. Quantitative Characterization of Surface Wettability by Friction Force. *Appl. Surf. Sci.* **2021**, *536*, No. 147788.

(36) Song, M.; Ju, J.; Luo, S.; Han, Y.; Dong, Z.; Wang, Y.; Gu, Z.; Zhang, L.; Hao, R.; Jiang, L. Controlling Liquid Splash on Superhydrophobic Surfaces by a Besicle Surfactant. *Sci. Adv.* **2017**, *3*, No. e1602188.

(37) Liu, Y.; Moevius, L.; Xu, X.; Qian, T.; Yeomans, J. M.; Wang, Z. Pancake Bouncing on Superhydrophobic Surfaces. *Nat. Phys.* **2014**, *10*, 515−519.

(38) Cannon, A. H.; King, W. P. Hydrophobicity of Curved Microstructured Surfaces. *J. Micromech. Microeng.* **2010**, *20*, No. 025018.

(39) Hsieh, H.-T.; Lin, V.; Hsieh, J.; Su, G. J. Design and Fabrication of Long Focal Length Microlens Arrays. *Opt. Commun.* **2011**, *284*, 5225−5230.

(40) Zhu, X.; Chen, H.; Zhu, L.; Wang, H.; Zhang, W. Fabrication of Curved Microlens Array Using a Drop-on-demand Droplet Generator and Polydimethylsiloxane Replica Mold. *Opt. Eng.* **2014**, *53*, No. 117109.

(41) Lin, V.; Wei, H.; Hsieh, H.; Su, G. J. An Optical Wavefront Sensor Based on a Double Layer Microlens Array. *Sensors* **2011**, *11*, 10293−10307.

(42) Wu, D.; Wu, S.-Z.; Niu, L.-G.; Chen, Q.-D.; Wang, R.; Song, J.-F.; Fang, H.-H.; Sun, H.-B. High Numerical Aperture Microlens Arrays of Close Packing. *Appl. Phys. Lett.* **2010**, *97*, No. 031109.

(43) Ristok, S.; Thiele, S.; Toulouse, A.; Herkommer, A. M.; Giessen, H. Stitching-free 3D printing of Millimeter-sized Highly Transparent Spherical and Aspherical Optical Components. *Opt. Mater. Express* **2020**, *10*, 2370−2378.

(44) Li, Z.; Lu, H.; Ding, Y.; Xu, M. Low Voltage Liquid Crystal Microlens Array based on Polyvinyl Alcohol Convex induced Vertical Alignment. *Liq. Cryst.* **2021**, *48*, 248−254.

(45) Deng, Z.; Chen, F.; Yang, Q.; Bian, H.; Du, G.; Yong, J.; Shan, C.; Hou, X. Dragonfly-Eye-Inspired Artificial Compound Eyes with Sophisticated Imaging. *Adv. Funct. Mater.* **2016**, *26*, 1995−2001.